

Supporting Information

Cu(II) complexes with a salicylaldehyde derivative and α -diimines as co-ligands: synthesis, characterization, biological activity. Experimental and theoretical approach

Snežana Selaković,^a Marko V. Rodić,^b Irena Novaković,^c Ivana Z. Matić,^d Tatjana Stanojković,^d Andrea Pirković,^e Lada Živković,^f Biljana Spremo-Potparević,^f Miloš Milčić,^g Vesna Medaković,^g Filitsa Dimiza,^h George Psomas,^h Katarina Anđelković^g, Maja Šumar-Ristović^g

^a University of Belgrade - Faculty of Pharmacy, Department of General and Inorganic Chemistry, 11000 Belgrade, Serbia

^b University of Novi Sad, Faculty of Sciences, Department of Chemistry, Biochemistry and Environmental Protection, 21102 Novi Sad, Serbia

^c University of Belgrade, Institute of Chemistry, Technology and Metallurgy, Department of Chemistry, 11000 Belgrade, Serbia

^d Institute of Oncology and Radiology of Serbia, Belgrade, Serbia

^e Institute for the Application of Nuclear Energy-INEP, Department for Biology of Reproduction

^f University of Belgrade - Faculty of Pharmacy, Department of Pathobiology, 11000 Belgrade, Serbia

^g University of Belgrade - Faculty of Chemistry, 11000 Belgrade, Serbia

^h Laboratory of Inorganic Chemistry, Department of Chemistry, Aristotle University of Thessaloniki, Thessaloniki GR-54124, Greece

Table of Contents

IR spectra characterization	S3
<i>In vitro</i> biological activity studies	S3
Binding study with CT DNA by UV spectroscopy	S3
CT DNA binding studies by cyclic voltammetry	S4
CT DNA-binding studies by viscosity measurements	S4
EB-displacement studies	S5
<i>In vitro</i> albumin binding studies	S6
Computational details	S7
EDA and QTAIM	S7
Table S1. Pertinent crystallographic and refinement details for 1 and 2	S8
Table S2. Results of EDA computations	S9
Table S3. Results of QTAIM analysis	S9
Fig. S1	S10
Fig. S2	S10
Fig. S3	S11
Fig. S4	S12
Fig. S5	S13
Fig. S6	S14
Fig. S7	S15
Fig. S8	S16
Fig. S9	S17
Fig. S10	S18
Fig. S11	S19
Fig. S12	S20
Fig. S13	S21
Fig. S14	S22
Fig. S15	S23
Fig. S16	S24
Fig. S17	S25
References	S26

IR spectra characterization

IR spectra of complexes **1** and **2** show that the phenol group of ligand HL in both complexes is coordinated deprotonated. The vibration of C-O bond in the HL ligand spectrum appears at 1214 cm⁻¹, while this band is shifted to higher wavenumbers in both complexes, 1454 cm⁻¹ for complex **1** and 1432 cm⁻¹ for complex **2**. Band on 1650 cm⁻¹, vibration of C=O bond of the aldehyde group of the free ligand HL, was shifted to lower frequencies, 1532 cm⁻¹ for complex **1** and 1524 cm⁻¹ for complex **2**. This indicates that ligand L additionally coordinates the copper ion through the oxygen of the aldehyde group, in both complexes. Intense bands in the spectrum of the complexes at 1619 cm⁻¹, for complex **1**, and 1622 cm⁻¹, for complex **2**, are assigned to the stretching vibrations of the $\nu(\text{C}=\text{N})$ group and indicate the coordination of the α -diimine ligand via nitrogen.

In vitro binding studies with CT DNA

Binding study with CT DNA by UV spectroscopy

UV-vis spectroscopy was used to study the interaction of the compounds with CT DNA in order to estimate their possible binding mode to CT DNA and calculate the corresponding binding constants. The UV spectra of CT DNA in the presence of each compound were recorded for a constant CT DNA concentration ($\sim 1.5 \times 10^{-4}$ M) at diverse [compound]/[CT DNA] ratios (r). Control experiments with DMSO were performed and no changes in the spectra of CT DNA were observed. The UV-vis spectra of the compounds were recorded for a standard concentration (2×10^{-5} – 1×10^{-4} M) in the absence or presence of an increasing concentration of CT DNA. The DNA-binding constant (K_b , in M⁻¹) can be obtained by monitoring the changes in the absorbance at the corresponding λ_{max} with increasing concentrations of CT DNA and it is given by the ratio of slope to the y intercept in plots [DNA]/($\epsilon_A - \epsilon_f$) versus [DNA], according to the Wolfe-Shimer equation¹:

$$\frac{[\text{DNA}]}{(\epsilon_A - \epsilon_f)} = \frac{[\text{DNA}]}{(\epsilon_b - \epsilon_f)} + \frac{1}{K_b(\epsilon_b - \epsilon_f)} \quad (\text{eq. S1})$$

where [DNA] is the concentration of DNA in base pairs, $\epsilon_A = A_{\text{obsd}}/[\text{compound}]$, ϵ_f = the extinction coefficient for the free compound and ϵ_b = the extinction coefficient for the compound in the fully bound form.

CT DNA binding studies by cyclic voltammetry

The interaction of complexes **1** and **2** with CT DNA was also investigated *via* monitoring the changes observed in the cyclic voltammogram of a 0.5 mM 1:2 DMSO:buffer solution of the complex upon the addition of DNA solution. The buffer was also used as the supporting electrolyte and the cyclic voltammograms were recorded at $\nu = 100 \text{ mV s}^{-1}$.

Cyclic voltammetry can be also used in order to calculate the corresponding equilibrium constant for the redox process. The ratio of the DNA-binding constants for the reduced (K_r) and oxidized forms (K_{ox}) of the complexes (K_r/K_{ox}) was calculated according to equation²:

$$\Delta E^{\circ} = E_{(b)}^{\circ} - E_{(f)}^{\circ} = 0.059 \times \log \frac{K_r}{K_{ox}} \quad (\text{eq. S2})$$

where $E_{(b)}^{\circ}$ and $E_{(f)}^{\circ}$ are the formal potentials of Cu(II)/Cu(I) couple in the fully bound and free complexes, respectively. K_{ox} and K_r are the binding constants for the binding of the oxidized and reduced species to DNA, respectively.

CT DNA-binding studies by viscosity measurements

The viscosity of DNA solution in buffer solution (150 mM NaCl and 15 mM trisodium citrate at pH 7.0) was measured upon increasing amounts of the compounds (up to the value of $r = 0.4$). All measurements were performed at room temperature and the obtained data are presented as $(\eta/\eta_0)^{1/3}$ *versus* r , where η is the viscosity of DNA in the presence of the compound and η_0 is the viscosity of DNA alone in buffer solution.

EB–displacement studies

Fluorescence emission spectroscopy was used to investigate the competitive studies of the compounds with EB for the DNA–intercalating sites (by displacing it from its DNA–EB conjugate). The CT DNA–EB complex was prepared by pre–treating 20 μM EB and 30 μM CT DNA in buffer (150 mM NaCl and 15 mM trisodium citrate at pH 7.0). The possible displacement of EB by the compounds and subsequently the intercalating effect was studied by the stepwise addition of a certain amount of a compound's solution into a solution of the DNA–EB conjugate. The effect of the addition of each compound to the DNA–EB solution was obtained by recording the variation of fluorescence emission spectra with excitation wavelength at 540 nm.³ The compounds do not show any appreciable fluorescence emission bands at room temperature in solution or in the presence of CT DNA or EB under the same experimental conditions ($\lambda_{\text{ex}} = 540 \text{ nm}$); therefore, the observed quenching of the EB–DNA solution may be attributed to the displacement of EB from its EB–DNA conjugate. The EB–displacement studies involved the calculation of the Stern–Volmer constant (K_{SV} , in M^{-1}) in order to evaluate the quenching efficiency of each compound according to the Stern–Volmer equation^{4,5}:

$$\frac{I_0}{I} = 1 + k_q \tau_0 [Q] = 1 + K_{\text{SV}} [Q] \quad (\text{eq. S3})$$

where I_0 and I are the emission intensities of the EB–DNA solution in the absence and the presence of the compound–quencher, respectively, $[Q]$ is the concentration of the quencher (i.e. compounds), $\tau_0 =$ the average lifetime of the emitting system without the quencher and $k_q =$ the quenching constant. K_{SV} was obtained from the Stern–Volmer plots by the slope of the diagram I_0/I versus $[Q]$. Taking $\tau_0 = 23 \text{ ns}$ as the fluorescence lifetime of the EB–DNA system,⁵ the quenching constants (k_q , in $\text{M}^{-1}\text{s}^{-1}$) of the compounds can be determined according to equation³:

$$K_{\text{SV}} = k_q \tau_0 \quad (\text{eq. S4})$$

***In vitro* albumin binding studies**

The albumin binding studies were performed by performing tryptophan fluorescence quenching experiments using bovine (BSA, 3 μ M) or human serum albumin (HSA, 3 μ M) in buffer solution. The quenching of the emission intensity of tryptophan residues of BSA at 345 nm or HSA at 340 nm was monitored using the compounds under study as quenchers with gradually increasing concentration and the fluorescence emission spectra were recorded in the range of 300–500 nm with excitation wavelength of 295 nm.³

The extent of the inner-filter effect can be roughly estimated with the following formula:

$$I_{\text{corr}} = I_{\text{meas}} \times 10^{\frac{\varepsilon(\lambda_{\text{exc}})cd}{2}} \times 10^{\frac{\varepsilon(\lambda_{\text{em}})cd}{2}} \quad (\text{eq. S5})$$

where I_{corr} = corrected intensity, I_{meas} = the measured intensity, c = the concentration of the quencher, d = the cuvette (1 cm), $\varepsilon(\lambda_{\text{exc}})$ and $\varepsilon(\lambda_{\text{em}})$ = the ε of the quencher at the excitation and the emission wavelength, respectively, as calculated from the UV-vis spectra of the compounds.⁶

The Stern-Volmer and Scatchard graphs are used in order to study the interaction of a quencher with serum albumins. According to Stern-Volmer quenching equation (eq. S4),³ where I_0 = the initial tryptophan fluorescence intensity of SA, I = the tryptophan fluorescence intensity of SA after the addition of the quencher (i.e. compounds), k_q = the quenching constant, K_{SV} = the Stern-Volmer constant, τ_0 = the average lifetime of SA without the quencher, $[Q]$ = the concentration of the quencher), K_{SV} (in M^{-1}) can be obtained by the slope of the diagram I_0/I versus $[Q]$, and subsequently the quenching constant (k_q , in $M^{-1}s^{-1}$) is calculated from eq. S5, with $\tau_0 = 10^{-8}$ s as fluorescence lifetime of tryptophan in SA.

The SA-binding constant (K , in M^{-1}) is calculated from the slope in plots $(\Delta I/I_0)/[Q]$ versus $\Delta I/I_0$ and n (the number of binding sites per albumin) is given by the ratio of y intercept to the slope all coming from the Scatchard equation^{3,7}:

$$\frac{\Delta I/I_0}{[Q]} = nK - K \frac{\Delta I}{I_0} \quad (\text{eq. S6})$$

Computational details

EDA and QTAIM

In EDA framework the interaction energy between fragments is decomposed into four chemically meaningful components: $E_{int} = E_{elst} + E_{Pauli} + E_{orb} + E_{disp}$. The term E_{elst} is the quasi-classical electrostatic interaction between the fragments; E_{Pauli} is the repulsive Pauli interaction between occupied orbitals on the two fragments; E_{orb} is a stabilizing contribution due to the charge transfer and polarization and, E_{disp} is the dispersion energy correction. The results of EDA calculations for crystal structure and BP86-D3BJ/Def2-TZVP optimized structure of complex 1 are shown in Table S2.

QTAIM analysis performed on BP86-D3BJ/Def2-TZVP optimized geometry of complex 1 reveals an (3,-1) Bond Critical Point between fluorine atom of BF_4^- fragment and Cu atom with low electron density and Laplacian of electron density values. In Table S3 properties of electron densities at BCPs between Cu atom and other ligating atoms in complex 1 are shown (Fig. S13).

Table S1. Pertinent crystallographic and refinement details for **1** and **2**

	1	2
Empirical formula	C ₁₉ H ₁₅ BCuF ₄ N ₂ O ₄	C ₂₁ H ₁₉ BCuF ₄ N ₂ O ₆
Formula weight	485.68	545.73
Temperature, K	295(2)	295(2)
Crystal system	triclinic	monoclinic
Space group (number)	<i>P</i> $\bar{1}$ (2)	<i>C</i> 2/ <i>c</i> (15)
<i>a</i> / Å	9.1227(2)	19.8478(6)
<i>b</i> / Å	10.2404(2)	16.7632(3)
<i>c</i> / Å	11.1777(2)	13.8843(4)
α / °	102.877(2)	90
β / °	104.810(2)	105.192(3)
γ / °	92.033(2)	90
<i>V</i> / Å ³	979.40(4)	4458.0(2)
<i>Z</i>	2	8
ρ_{calc} / g cm ⁻³	1.647	1.626
μ / mm ⁻¹	1.182	1.055
<i>F</i> (000)	490	2216
Crystal color	green	green
Crystal shape	plate	block
Radiation	MoK α (λ =0.71073 Å)	MoK α (λ =0.71073 Å)
2 θ range, °	4.1 to 52.7 (0.80 Å)	4.0 to 58.5 (0.73 Å)
Reflections collected	16006	17134
Independent reflections	4009	5286
	$R_{\text{int}} = 0.021$	$R_{\text{int}} = 0.021$
	$R_{\text{sigma}} = 0.016$	$R_{\text{sigma}} = 0.021$
Completeness	100 %	100 %
Data / Restraints / Parameters	4009/66/309	5285/35/336
Goodness-of-fit on <i>F</i> ²	1.028	1.043
Final <i>R</i> indexes	$R_1 = 0.033$	$R_1 = 0.037$
[$I \geq 2\sigma(I)$]	$wR_2 = 0.088$	$wR_2 = 0.097$
Final <i>R</i> indexes	$R_1 = 0.037$	$R_1 = 0.047$
[all data]	$wR_2 = 0.091$	$wR_2 = 0.103$
Largest peak/hole, e Å ⁻³	0.52/−0.35	0.38/−0.28

Table S2. Results of EDA computations^a

[Cu(bipy)(L)BF ₄]	E _{elst}	E _{Pauli}	E _{orb}	E _{disp}	E _{tot}	Δq ^b
Crystal structure ^c	-72.45	21.60	-16.52	-5.48	-72.85	0.08
Optimized geometry ^d	-72.27	18.95	-16.37	-5.95	-75.64	0.08

^aAll the energies are in kcal/mol; ^bHirshfeld charge transfer between fragments; ^cCoordinates taken from crystal structure and wavefunction calculated at BP86-D3BJ/Def2-TZVP level of theory; ^dcalculation on BP86-D3BJ/Def2-TZVP optimized structure.

Table S3. Results of QTAIM analysis

Contact	ρ(r _c)	∇ ² (r _c)
Cu ---F	0.0262	0.1241
Cu ---O1	0.0849	0.3923
Cu ---O2	0.0934	0.4290
Cu ---N1	0.0890	0.3231
Cu ---N2	0.0901	0.3294

Table S4. Coefficients of selectivity (Cs) in the cytotoxic activity of Cu(II) complexes and their precursor compounds as a ratio of the IC₅₀ values for normal human keratinocytes HaCaT and human malignant cell lines

	HaCaT/HeLa	HaCaT/A375	HaCaT/PC-3	HaCaT/MCF7	HaCaT/A549
1	1.08	1.65	1.20	0.88	0.82
2	0.97	0.94	0.91	0.72	0.70
HL	1.45	1.62	1.48	0.54	≈0.37
bipy	0.42	0.86	0.48	>0.20	0.22
phen	0.62	0.68	0.65	0.14	0.53
Cu(BF ₄) ₂ · 6H ₂ O	0.75	0.83	0.95	0.93	0.58
Cisplatin	0.56	0.91	0.18	0.13	0.18

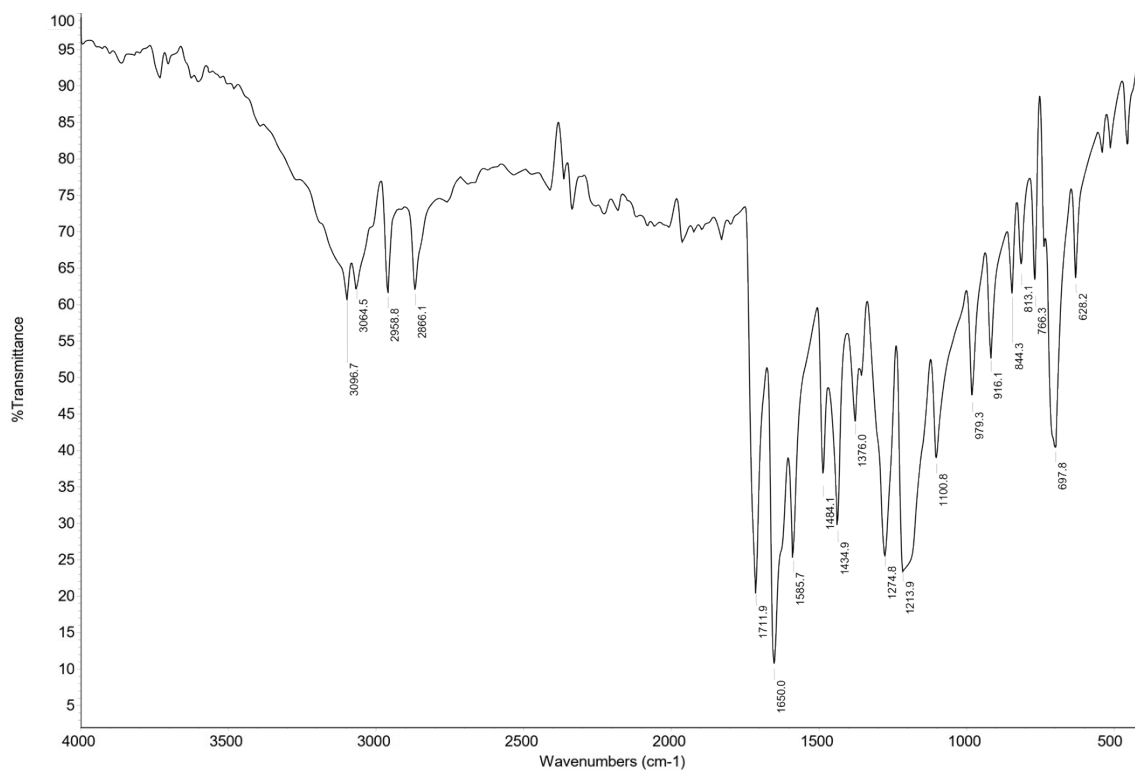


Fig. S1. IR spectra of methyl 3-formyl-4-hydroxybenzoate (HL)

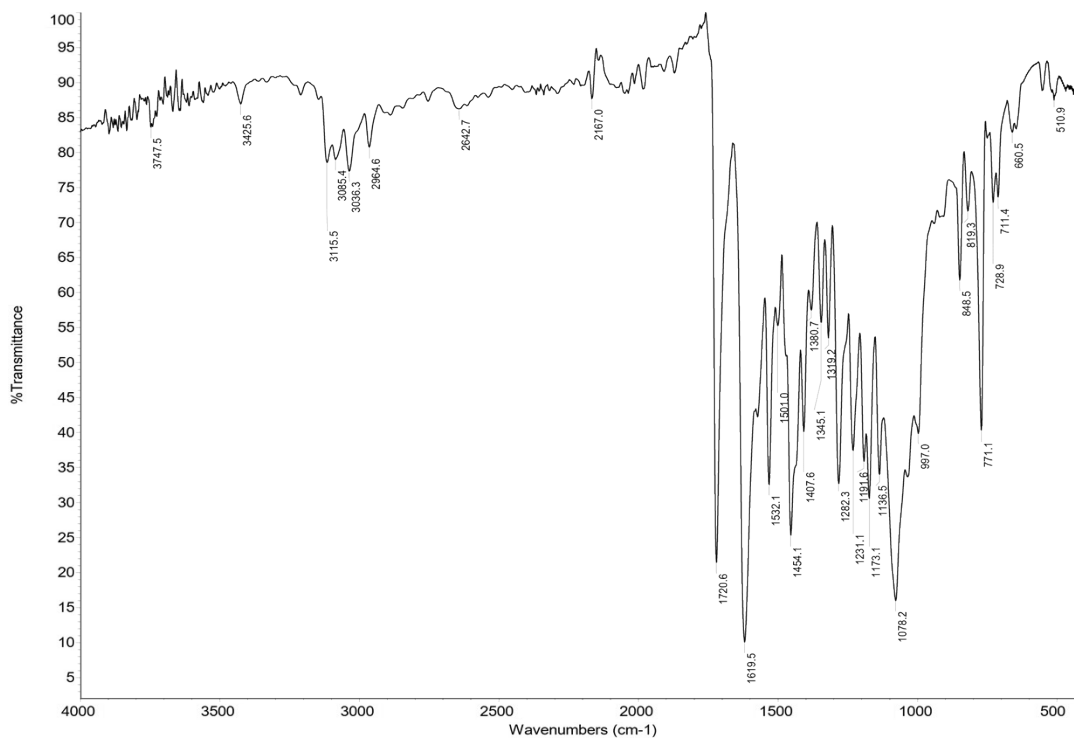


Fig. S2. IR spectra of complex [Cu(bipy)(L)(BF₄)] (1)

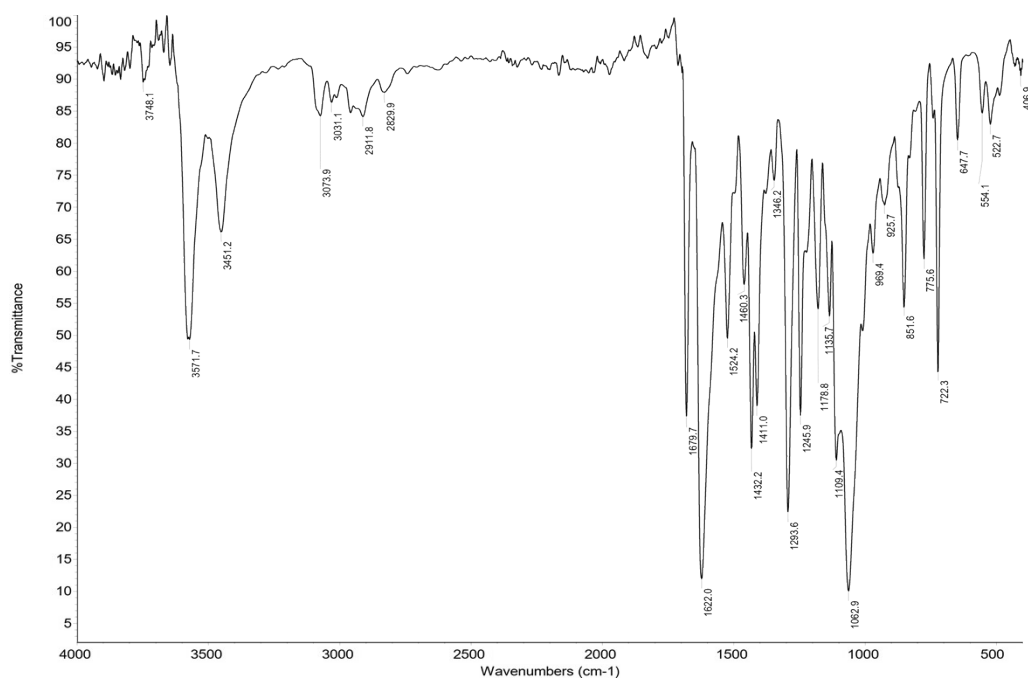
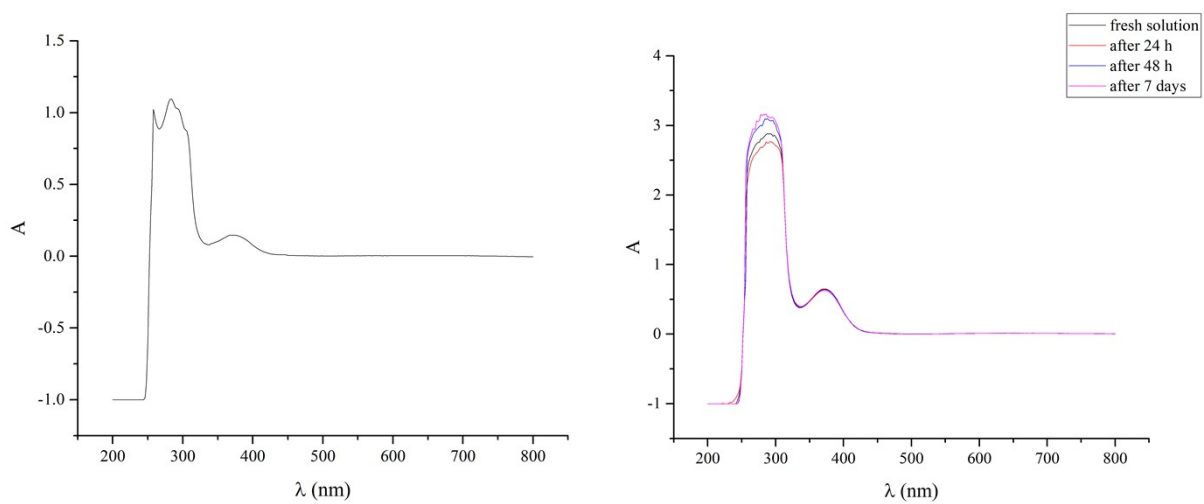
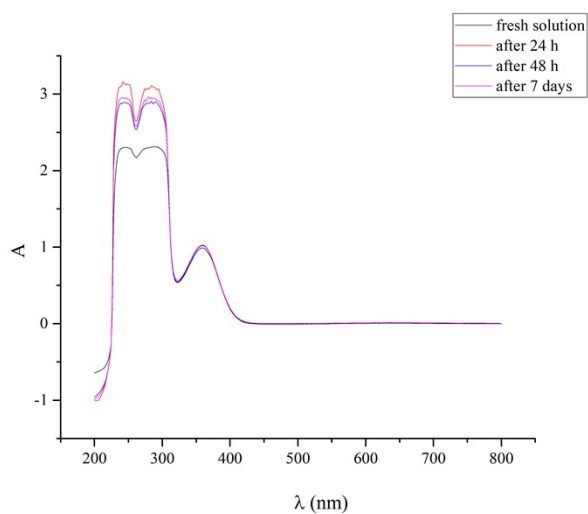


Fig. S3. IR spectra of complex $[\text{Cu}(\text{phen})(\text{L})(\text{H}_2\text{O})](\text{BF}_4) \cdot \text{H}_2\text{O}$ (**2**)



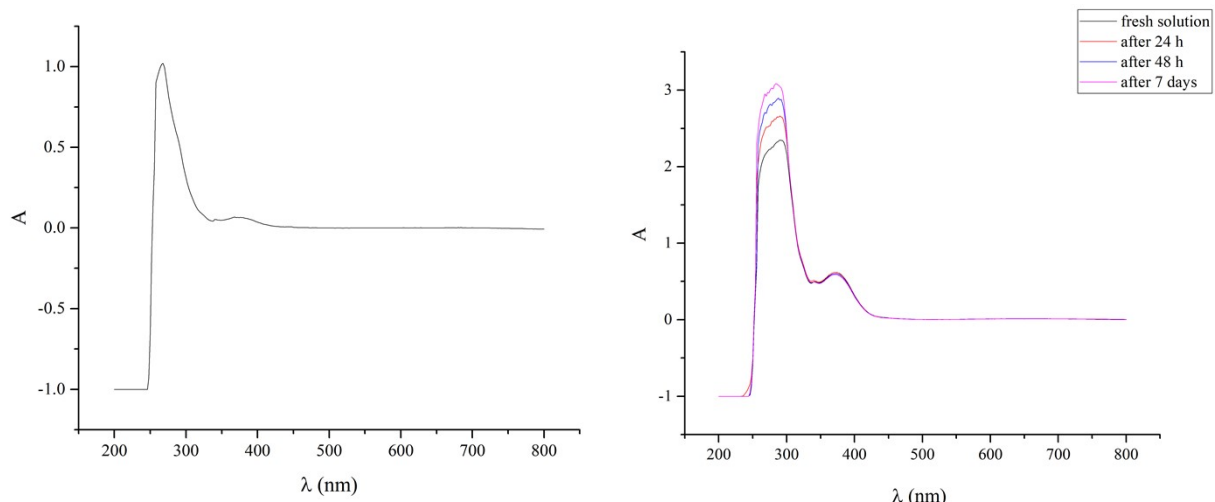
(A)

(B)



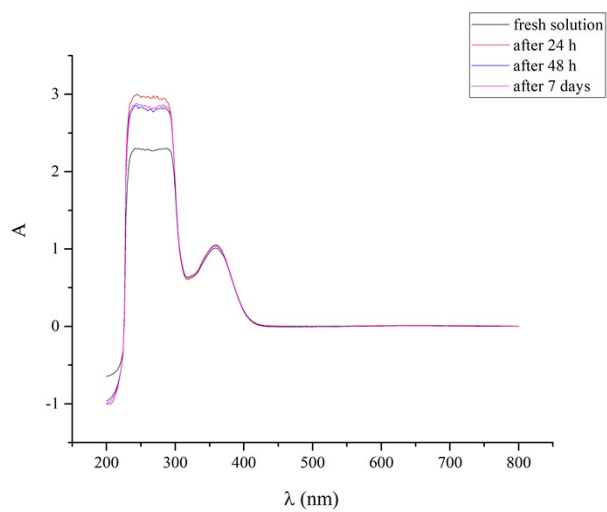
(C)

Fig. S4. UV-vis spectra of a (A) DMSO solution of complex **1** (5×10^{-5} M), (B) DMSO solution of complex **1** (2×10^{-4} M), and (C) PBS solution of complex **1** (2×10^{-4} M).



(A)

(B)



(C)

Fig. S5. UV-vis spectra of a (A) DMSO solution of complex **2** (2.5×10^{-5} M), (B) DMSO solution of complex **2** (2×10^{-4} M), and (C) PBS solution of complex **2** (2×10^{-4} M).

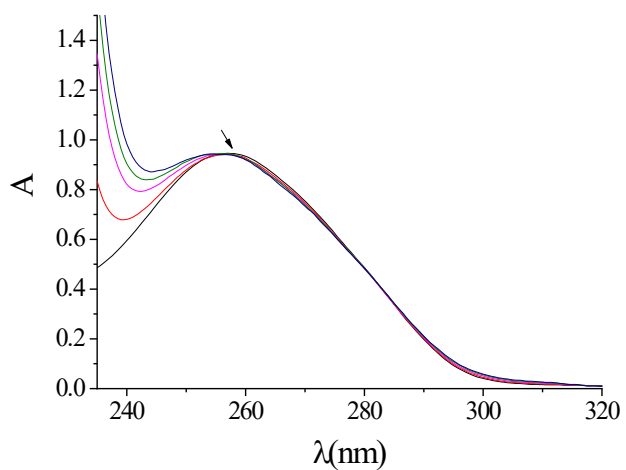


Fig. S6. UV-vis spectra of a solution of CT DNA ($[DNA] = 1.5 \times 10^{-4}$ M) in buffer solution (150 mM NaCl and 15 mM trisodium citrate at pH 7.0) in the presence of increasing amounts of complex **1** (up to 1×10^{-4} M). The arrow shows the changes upon increasing amounts of complex **1**.

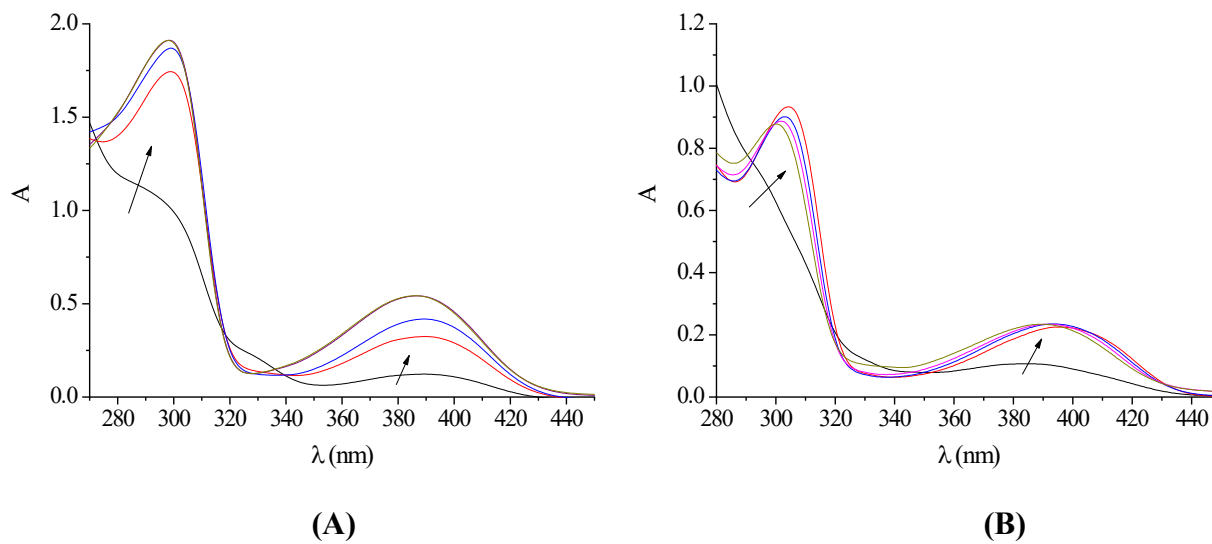
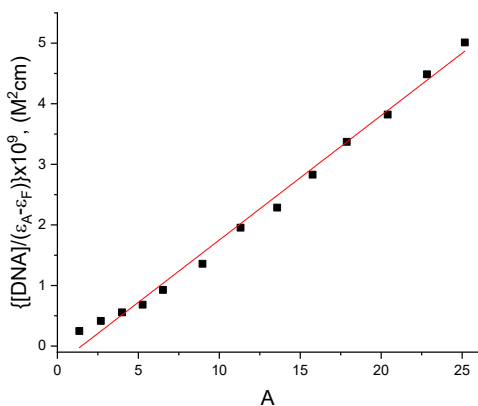
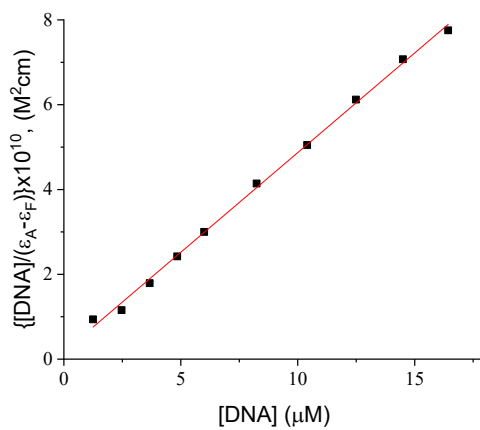


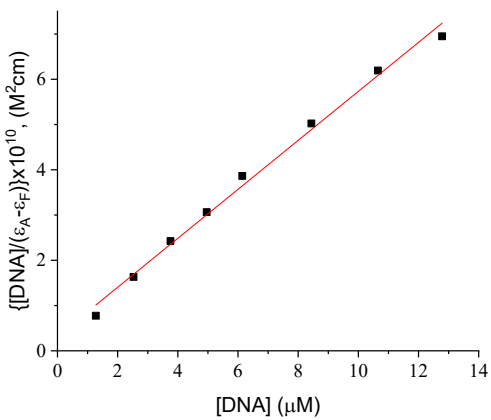
Fig. S7. UV-vis spectra of a DMSO solution of (A) HL (1×10^{-4} M) and (B) complex **2** (2×10^{-5} M), in the presence of increasing amounts of CT DNA. The arrows show the changes upon increasing amounts of CT DNA.



(A)



(B)



(C)

Fig. S8. Plot of $[\text{DNA}]/(\epsilon_A - \epsilon_F)$ versus [DNA] for (A) HL, (B) complex 1, and (C) complex 2.

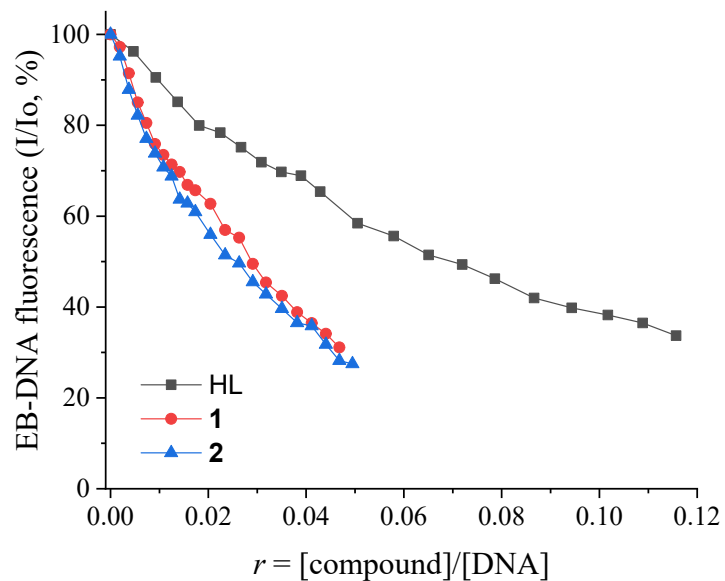
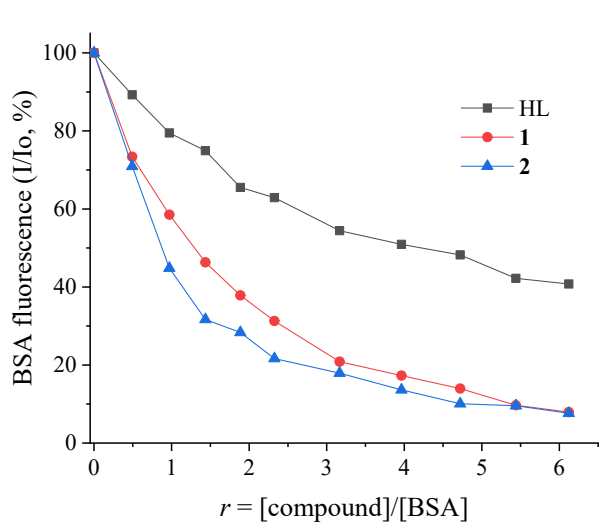
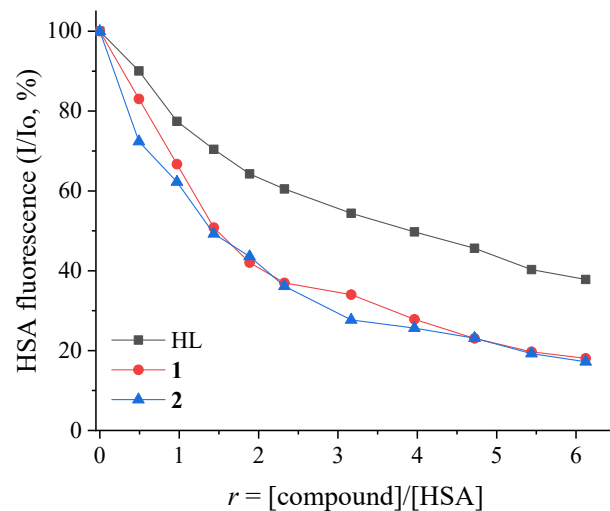


Fig. S9. Plot of relative EB–DNA fluorescence emission intensity at $\lambda_{\text{emission}} = 592 \text{ nm}$ (I/I_0 , %) versus r ($r = [\text{complex}]/[\text{DNA}]$) (up to 33.7 % of the initial EB–DNA fluorescence intensity for HL, 31.1% for complex **1**, and 27.5% for **2**).

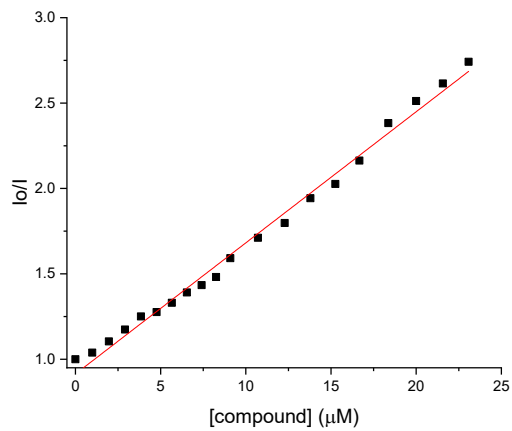


(A)

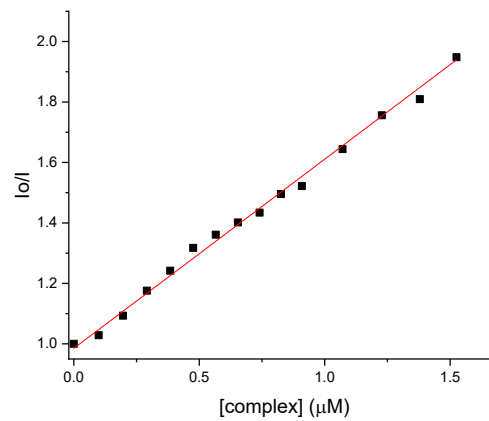


(B)

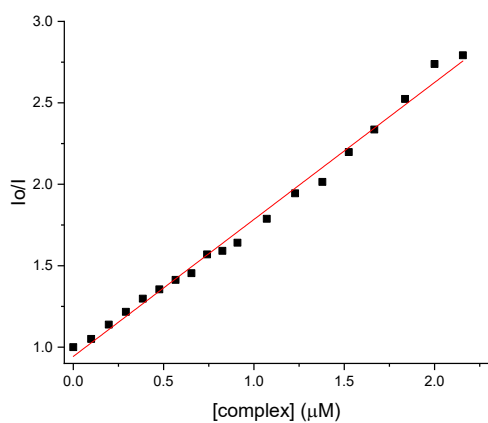
Fig. S10. (A) Plot of relative fluorescence emission intensity of BSA at $\lambda_{em} = 344$ nm (I/I_0 , %) versus r ($r = [\text{complex}]/[\text{BSA}]$) for the compounds (up to 40.7% of the initial BSA fluorescence for HL, 8.0% for complex **1** and 7.7% for **2**) in buffer solution (150 mM NaCl and 15 mM trisodium citrate at pH 7.0). (B) Plot of relative fluorescence emission intensity of HSA at $\lambda_{em} = 340$ nm (I/I_0 , %) versus r ($r = [\text{complex}]/[\text{HSA}]$) for the compounds (up to 37.8% of the initial HSA fluorescence for HL, 18.1% for complex **1** and 17.2% for **2**) in buffer solution (150 mM NaCl and 15 mM trisodium citrate at pH 7.0).



(A)

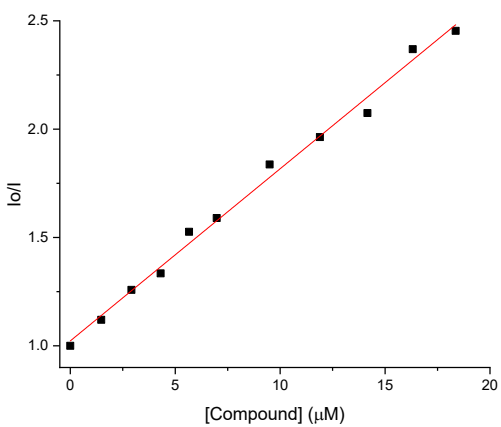


(B)

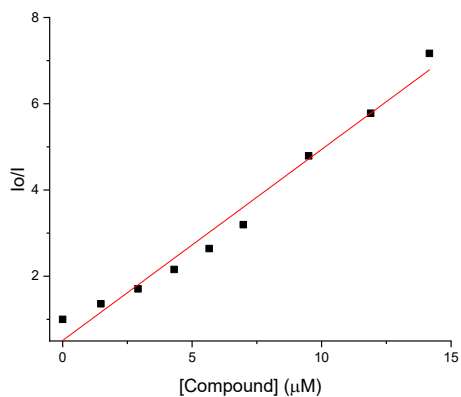


(C)

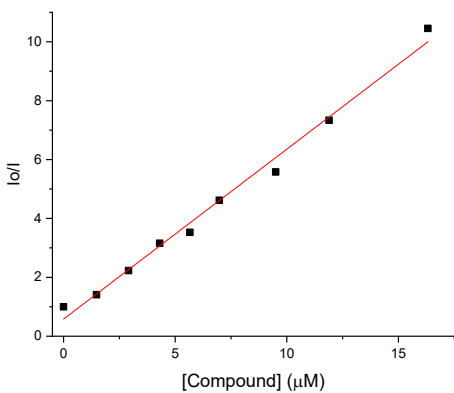
Fig. S11. Stern–Volmer quenching plot of the EB–DNA fluorescence in the presence of (A) HL, (B) complex 1 and (C) complex 2.



(A)

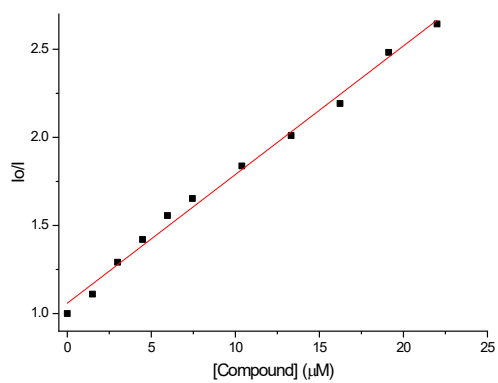


(B)

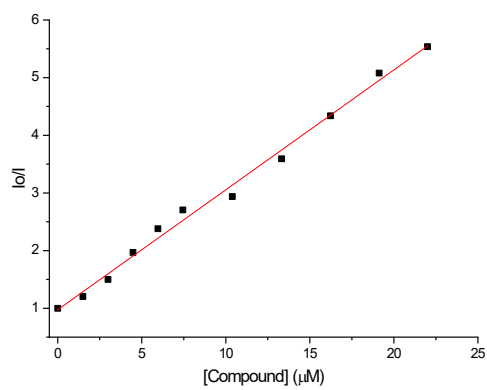


(C)

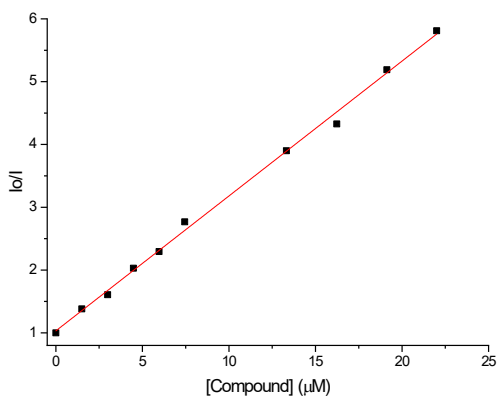
Fig. S12. Stern–Volmer quenching plot of the BSA fluorescence in the presence of (A) HL, (B) complex 1, and (C) complex 2.



(A)

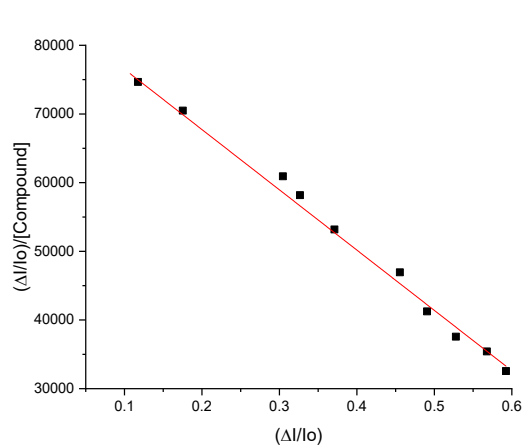


(B)

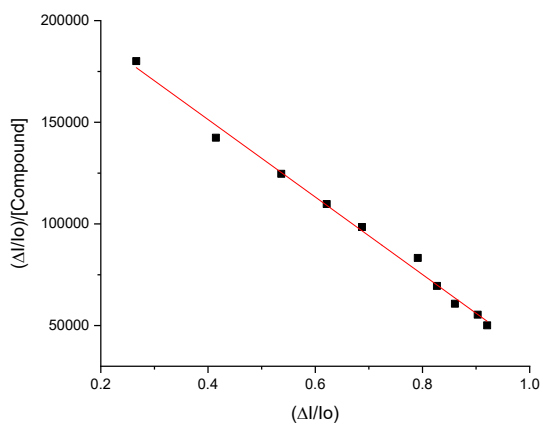


(C)

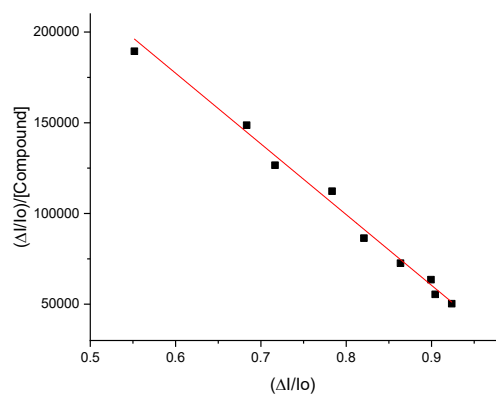
Fig. S13. Stern–Volmer quenching plot of the HSA fluorescence in the presence of (A) HL, (B) complex **1**, and (C) complex **2**.



(A)

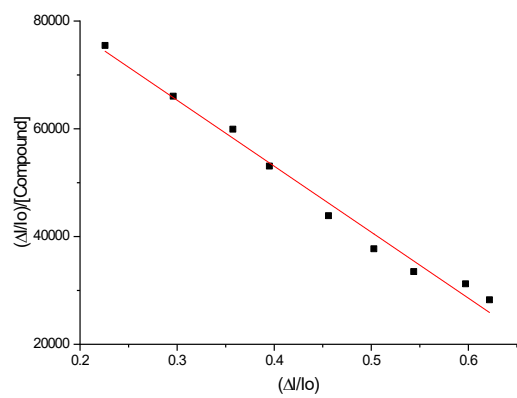


(B)

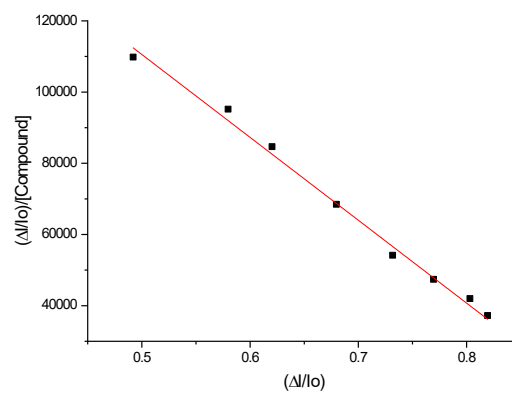


(C)

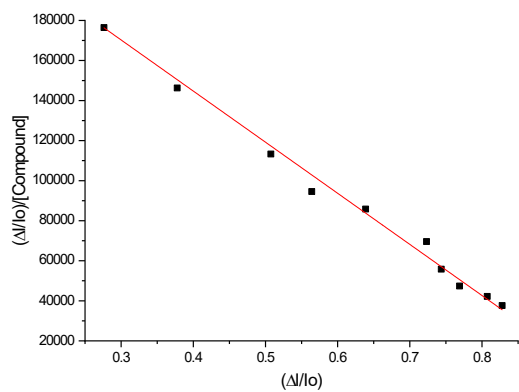
Fig. S14. Scatchard plot of BSA in the presence of (A) HL, (B) complex 1, and (C) complex 2.



(A)



(B)



(C)

Fig. S15. Scatchard plot of HSA in the presence of (A) HL, (B) complex 1, and (C) complex 2.

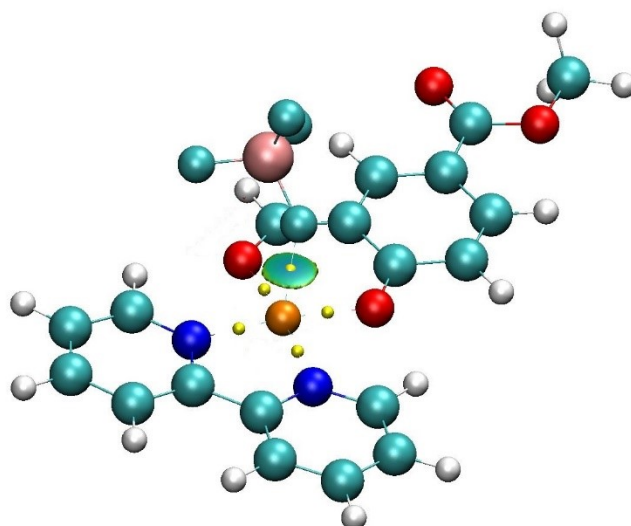


Fig. S16. Bond Critical Points (yellow spheres) between Cu(II) and ligating atoms in complex 1. Green surface – NCI index for Cu(II) – F interaction.

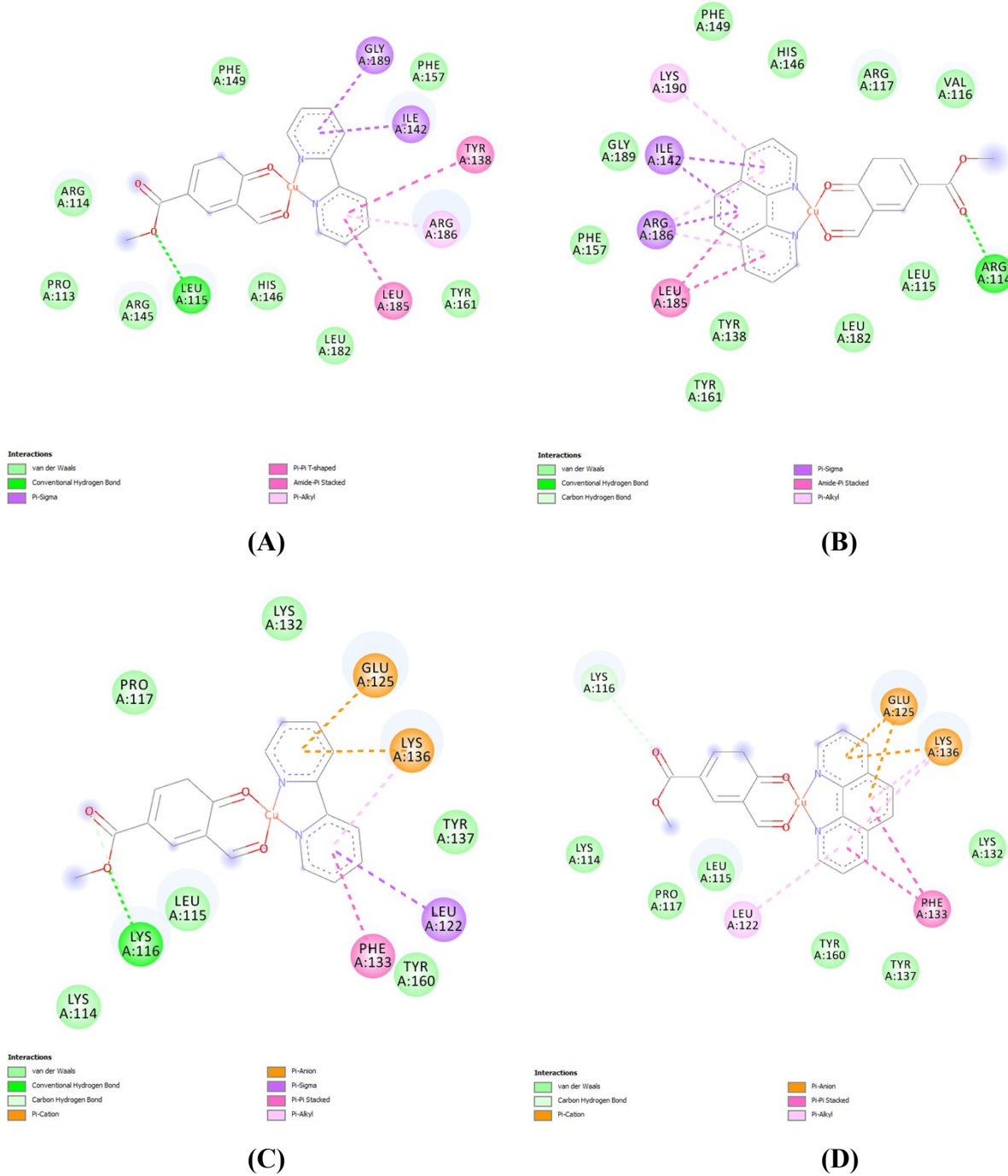


Fig. S17. 2D interaction diagram for binding of square-planar derivative of a) complex 1 to HSA; b) complex 2 to HSA; c) complex 1 to BSA and d) complex 2 to BSA

References

- 1 A. Wolfe, G. H. Shimer and T. Meehan, *Biochemistry*, 1987, **26**, 6392–6396.
- 2 M. T. Carter, M. Rodriguez and A. J. Bard, *J. Am. Chem. Soc.*, 1989, **111**, 8901–8911.
- 3 J. R. Lakowicz, *Principles of Fluorescence Spectroscopy*, Springer US, Boston, MA, 2006.
- 4 G. Zhao, H. Lin, S. Zhu, H. Sun and Y. Chen, *J. Inorg. Biochem.*, 1998, **70**, 219–226.
- 5 D. P. Heller and C. L. Greenstock, *Biophys. Chem.*, 1994, **50**, 305–312.
- 6 L. Stella, A. L. Capodilupo and M. Bietti, *Chem. Commun.*, 2008, 4744.
- 7 Y.-Q. Wang, H.-M. Zhang, G.-C. Zhang, W.-H. Tao and S.-H. Tang, *J. Lumin.*, 2007, **126**, 211–218.